4D MULTI-SCALE IMAGING OF REACTION IN CARBONATES: THE IMPACT OF HETEROGENEITY ON DISSOLUTION REGIMES AT THE CORE AND PORE SCALES WITH APPLICATIONS TO CO_2 STORAGE

Menke, H.P.[1]; Reynolds, C.A.[1]; Andrew M.G.[2]; Bijeljic, B.[1]; Blunt, M.J.[1]

[1]Imperial College London, Department of Earth Science & Engineering, London SW7 2AZ, UK
[2]Carl Zeiss X-ray Microscopy Ltd, 4385 Hopyard Rd #100, Pleasanton, CA 94588, USA

This paper was prepared for presentation at the International Symposium of the Society of Core Analysts held in Snowmass, Colorado, USA, 21-26 August 2016

ABSTRACT

Understanding how to upscale pore scale rock-fluid interaction processes for predictive modelling poses a significant challenge to the carbon storage and petroleum industries. We have designed a set of experiments to investigate the impact of scale and pore-space heterogeneity on the dissolution of two carbonates at both the pore and core scales. Two rock samples were reacted with reservoir condition CO_2 saturated brine at the two different scales and scanned dynamically as dissolution took place. First, 1-cm long 4-mm diameter micro cores were scanned during reactive flow at a 4-μm resolution between 4 and 40 times using 4D X-ray micro-tomography over the course of 1.5 hours using a laboratory μ-CT. Second, 3.8-cm diameter, 8-cm long macro cores were reacted at the same conditions inside a reservoir condition flow rig and imaged using a medical CT scanner. Each sample was imaged ~13 times over the course of 1.5 hours at a 250 x 250 x 500-μm resolution. The reacted macro cores were then scanned inside a μ-CT at a 27-μm resolution to assess the alteration in pore-scale reaction-induced heterogeneity. It was found that both rock types showed channel formation at the pore-scale and progressive high porosity pathway dissolution at the core-scale with the more heterogeneous rock having faster dissolution progressing along direction of flow. Additionally, upon analysis of the high-resolution macro core images it was found that the dissolution pathways contained a distinct microstructure that was not visible at the resolution of the medical CT, where the reactive fluid had not completely dissolved the internal pore-structure. This microstructure was further analysed for connected pathway channel frequency and cross-sectional area. It was found that the frequency of channels decreased and the total cross sectional area increased with increasing pore-space heterogeneity. However, the average area per channel remained constant. This work represents the first study of scale dependence using reservoir condition 4D X-ray tomography and provides insight into the mechanisms that control local reaction rates at multiple scales.

INTRODUCTION

A major concern in the implementation of carbon capture and storage (CCS) is long-term storage security [1, 2]. Carbon dioxide, CO_2, injected into the subsurface will dissolve in the resident brine and form carbonic acid [3-5]. Carbonate host rocks have the potential to react with and be dissolved by CO_2 acidified brine [6]. Dissolution of the host rock may instigate unpredictable fluid flow and can weaken carbonate cements and damage injection wells [7, 8]. Therefore, it is important to have a complete understanding of dissolution in the brine-rock system to predict the distribution and the rate of fluid movement and the amount and impact of dissolution in the subsurface [9-11].

However, the nature and rate of dissolution in carbonates is dependent on both the properties of the brine [12-14] and the host rock [15, 16]. Carbonate dissolution rates are also strongly dependent on brine temperature and pressure [6], making it necessary to develop experimental techniques to measure complex time-dependent processes at representative reservoir conditions. Additionally, different dissolution regimes have been observed depending on flow and reactive conditions [13, 17] including wormholing, uniform, and face dissolution.

In subsurface research, it is common to use core-flooding techniques coupled with three-dimensional imaging to investigate reaction at the fluid/solid boundary. A commonly used imaging technique is computed tomography (CT), which can operate at different scales. Medical CT scanners [18] are commonly paired with core-flooding to image rocks at the core (~cm) scale. Core–scale imaging is valuable because it is three-dimensional and can be temporally resolved. However, it has a maximum resolution of, at best, ~100 μm and thus can only resolve the fluid/solid boundary of large features such as fractures and vugs. The greater portion of the pore space is only resolved as an average greyscale value as several pores or parts of pores will be contained in a single voxel, thus making segmentation and analysis of local changes in connectivity and reaction rate very difficult. X-ray microtomography (μ-CT) [19] provides higher resolution, and although it can only image *mm*-scale samples, it is ideal for resolving μm-scale processes. However, due to the small sample size μ-CT does not always capture the full range of physical heterogeneities seen at the core scale.

Imaging of dissolution in limestone rock has been performed at the core (*~cm*) scale using CT scanning. Ott et al [20] investigated dissolution using core flooding and CT scanning where, for several rock types and flow regimes, it was found that reaction of the dissolved CO_2 with the solid matrix increased physical heterogeneity. Ellis et al. [21] used core-scale imaging to show that exposure to CO_2 progressively reduced the sealing capacity of fractured claystone caprocks. Smith et al. [22] imaged dissolution of a dolomitic core before and after reaction with CO_2 acidified brine. Lamy-Chappuis et al. [23] used CT scanning to measure calcite dissolution in calcareous gritstone and found that the permeability increase with porosity did not agree with classical models and that the dissolution rate was impacted largely by the acid supply.

There are relatively few experiments that investigate the impact of coupled dissolution and flow phenomena at the micron scale (~μm) – the observation scale that is necessary for pore-scale analysis and numerical simulations of both flow and transport. Noiriel et al. [24] used μ-CT to measure the three-dimensional changes in a limestone fracture at several locations along the fracture during acid dissolution at ambient conditions. Additionally, Noiriel et al. [25] showed a power law relationship between

porosity and permeability during limestone dissolution by scanning the rock periodically *ex situ*. Menke et al. [26] imaged the dissolution dynamics of a relatively homogeneous carbonate at reservoir conditions while Menke et al. [27] used fast synchrotron tomography to image dissolution in two heterogeneous carbonates at two flow rates. They found that the porosity can either increase uniformly through time along the length of the samples, or may exhibit a spatially and temporally varying increase that is attributed to channel formation. Channelling is the widening of fast flow pathways through the rock in a flow regime where the injected acid penetrates throughout the rock. This is distinct from wormholing, seen at faster reaction rates, where the injected acid etches a hole through the sample, and the injected acid is confined to this hole.

However, to date no studies have investigated the scale dependence of reaction-induced changes in pore structure. The main goal of this study is to investigate how different transport and reaction conditions alter complex pore structures at the pore and core scales by comparing dynamic reaction-induced changes in pore-space geometry and topology, and flow in subsurface rock systems at reservoir temperatures and pressures.

SAMPLE CHARACTISATION

Two samples of carbonate rock were chosen for these experiments, Ketton and Portland basebed. Both are oolitic limestones made of >97.1 % calcite with a minor quartz component. Ketton was deposited 169-176 million years ago and is quarried in Ketton, Rutland, UK. It is an almost pure calcite medium-grained oolite with microporous cement with a standard micritic texture. Portland Basebed is quarried in Portland, UK and was deposited during the Jurassic age. It is a fine-grained grainstone containing tightly packed ooids with interparticular porosity and microporous cement. Figure 5B depicts the normalised porosity distribution for our samples. Ketton has a wider, but shorter distribution than Portland with a peak at slightly higher porosity. Figure 5C shows the normalised pore size distributions (C) for Ketton (blue) and Portland (red) derived from mercury injection capillary pressure (MICP) tests. The image resolution limits for 4 μm (solid) and 27 μm (dashed) show that our imaging resolutions are likely to capture the largest pore throats for segmentation, but are unlikely to capture the constraints on the smallest flow pathways, especially in Portland which has much narrow pore throats than Ketton. At the resolution of the medical CT scanner of 250 μm, no segmentable initial pore structures are likely to be captured. Menke et al. [26, 27] performed network extractions at the pore scale for Ketton and Portland and found that Ketton is very well connected with a homogenous pore structure while Portland is poorly connected with a highly heterogeneous pore structure.

EXPERIMENTAL METHODS

Two experimental apparatuses were used to image dynamic dissolution in our samples. Figure 2A depicts the apparatus used for the mm-scale experiments and Figure 2B depicts the apparatus used for the cm-scale experiments. The Zeiss Versa XRM-500 *μ*-CT scanner and the Diamond Lightsource pink beam were used to image reaction between calcite and CO_2 saturated brine at reservoir conditions (50^oC and 10 MPa). Using our *in situ* apparatus [Figure 1], carbonate cores of ~1 cm length and 4 mm diameter of Ketton and Portland Basebed limestone were reacted by injecting

supercritical (sc) CO_2 saturated brine (pH 3.1) at a flow rate of 0.1 $mL.min^{-1}$. These microcores were imaged between 4 and 40 times over the course of 1.5 hours at a resolution of 4 μm. The precise details of the experimental apparatus and method are described in [27] for the Portland experiment and [28] for the Ketton experiment.

These experiments were then repeated at the core scale using cores that were drilled from the same 1 m^3 blocks as in the previous experiments. Cores of Ketton and Portland, ~8 cm long and 3.8 cm in diameter, were reacted with CO_2 saturated brine using the core scale experimental apparatus by injecting pH 3.1 brine at a flow rate of 9 $mL.min^{-1}$. This flowrate was chosen to keep the flow conditions identical at both experimental scales and thus the Darcy velocity, or flowrate per unit area was the same for the micro and macro scale experiments. The macro cores were imaged using a medical CT scanner ~13 times over the course of 1.5 hours with a 250 × 250 × 500 μm voxel size. The experimental apparatus is the same as detailed in [29]. Furthermore, the entirety of each macro core was imaged post-reaction in a Zeiss XRM-520 using automated stitching of a sequence images acquired along the axis of the core employing a flat panel detector at a 27 μm resolution to create a high resolution volume of 1400 × 1400 × 3000 voxels where the internal pore structure is both visible and able to be segmented for quantitative analysis.

All images were then post-processed using the image processing modules in Avizo 9.1 (www.vsg.com). The high-resolution micro-scale images were filtered and segmented and the porosity measured. The permeability was assessed using a Navier-stokes solver used in [27]. The low-resolution dynamic core scale images acquired using a medical CT were analyzed for porosity by the method presented in [30] while the permeability was measured experimentally using the pressure drop across the core [29]. Finally, the high-resolution images acquired by μ-CT were filtered and segmented and analysed for connected pathways and channel frequency and cross-sectional area.

PORE SCALE DYNAMICS

Figure 2 depicts the evolution of porosity, permeability and velocity for Ketton (A) and Portland (B) micro-cores over the course of 90 minutes of dissolution. Both cores exhibit channel formation where there is no discernable difference in dissolution rate along the direction of flow, but show a large initial increase in porosity as the high permeability channels expand followed by a smaller increase at later times after the channels are established. Ketton has many channels initially and shows a small increase in permeability of one order of magnitude during the experiment, while Portland has a few initial channels and has a permeability increase of over five orders of magnitude with the largest increase at early times during the channel formation stage. During the later stage of both experiments the permeability increases during a small widening of the flow pathways, but the corresponding porosity increase is nearly imperceptible.

The number of pore volumes of fluid and the Péclet (*Pe*) and Péclet-Damköhler (*PeDa*) were calculated for each rock. As expected the *Pe* number decreased as porosity increased during each experiment. However, the *PeDa* remained relatively constant and was <<1. The number of pore volumes (*PV*) approached 700 for each experiment suggesting that the reactions are not fluid limited.

CORE SCALE DYNAMICS

Figure 3 depicts the evolution of porosity and permeability for Ketton (A) and Portland (B) macro-cores over the course of 90 minutes of dissolution. Both cores exhibit large increases in porosity near the sample inlet which progress along the length of the cores during the experiment. The high porosity region is narrower for Portland and extends more quickly, while Ketton has a wider high porosity region that extends more slowly. Both cores show the largest increase in porosity in the regions with the highest initial porosity and the progression of dissolution tends to extend sequentially through time into the higher porosity regions further along the core. The increase in total porosity is similar (~0.04) for both cores. The permeability of the Ketton core shows no change while the permeability of the Portland core increases by two orders of magnitude. The spatial distribution of porosity increase suggests that the Portland core experienced breakthrough of the widening channels to the outlet of the core while the Ketton channels terminated before the end of the core.

The *Pe*, *PeDa*, and *PV* were calculated for each experiment. The *Pe* number decreased as porosity increased during each experiment and was approximately similar to the pore scale experiments. The *PeDa* also remained relatively constant, was in good agreement with the pore scale experiments and was <<1. The number of pore volumes (PV) approached 50 for each experiment, which is smaller than the pore scale experimental value of 700 PV (due to the core scale samples being ~20x longer that the pore scale samples proportional to the cross sectional area), but still suggests that the reactions are not fluid limited.

POST-REACTION HIGH RESOLUTION CORE-SCALE IMAGING

The entirety of each macro core was imaged post-reaction using automated stitching of a sequence of images acquired along the axis of the core using a flat panel detector at 27 μm resolution to create volume of 1400 × 1400 × 3000. The images were then processed and segmented and the pore structure was extracted [Figure 4A-B]. Ketton showed an even distribution of pore space while Portland had distinct channels. Furthermore, the pore space was analyzed for connectivity [Figure 4C-D] and it was found that at this resolution the pore space of Ketton was reasonably well-connected with small areas of disconnection while Portland exhibited four disconnected channels sets that were connected within each set but disconnected from each other and were accompanied by many small regions of entirely disconnected porosity. In Ketton, which typically has large pores and throats, connected pore space at this resolution was observable even before dissolution, while in Portland channels were only visible where dissolution had taken place. Portland is a lower permeability rock that typically has smaller pore throats and thus the image resolution was not sufficient to capture the connectivity of the pore space.

The connected pore space of each image was then analyzed for connected paths along the direction of flow for both the macro scale and micro scale images. The number of paths in each individual slice perpendicular to the flow axis [Figure 5A] were counted and the cross sectional area was measured [Figure 5D-E]. In the macro scale images [Figure 5D] the total number of channels remained relatively constant in Ketton while

Portland had fewer channels with a constant frequency in each slice along the connected flow axis, but the frequency decreased towards the outlet of the core. The total channel area was higher overall for Ketton than Portland corresponding to the higher overall porosity. Ketton had a larger area near the inlet and then constant area along the rest of the length of the core while Portland showed a steady, but slow decline with distance from the sample inlet. However, the average cross sectional area per channel was remained relatively constant along the length of each core with Ketton showing a small uptick near the sample inlet. The maximum channel width was highest for Ketton near the inlet, which then stabilised at later time, while the Portland had a steady width for the length of the channels. The higher maximum channel area in Ketton may be due to channels merging where large of amounts of dissolution have occurred near the inlet.

In the microscale images [Figure 5E] Portland had a greater number of channels than Ketton, but the channels were on average smaller. However, Ketton had a larger total channel cross sectional area due to a larger proportion of the porespace contributing to the connected porosity (visualized in blue in Figure 5D-E). There was no discernable spatial variation of maximum channel area along the axis of flow for either rock type.

CONCLUSIONS

We have imaged the dissolution of Portland and Ketton carbonates at the same flow and reactive conditions at the micro and macro core scales. We find that evolution of porosity is structure dependent and that porosity evolution perpendicular to the axis of flow behaves similarly across scales, but that along the axis of flow the micro-scale does not capture the heterogeneous porosity propagation visible at the macro scale. Additionally, we find that the permeability evolution is structure dependent, but well captured across both the micro and macro scales. Moreover, at the macro scale we find that the maximum cross-sectional area per channel is scale dependent, but that the frequency of channels was not structure dependent and the average cross sectional area decreased with increasing pore-space heterogeneity. This work represents the first study of scale dependence using in situ 4D tomography and provides insight into the mechanisms that control local reaction rates at the *mm* and *cm* scales. Furthermore, this work implies that at the field scale under these conditions it is structural heterogeneities rather than fluid limitations that dominate dissolution and therefore the evolution of high permeability pathways.

ACKNOWLEDGEMENTS

We gratefully acknowledge funding from the Qatar Carbonates and Carbon Storage Research Centre (QCCSRC), provided jointly by Qatar Petroleum, Shell, and Qatar Science & Technology Park.

REFERENCES

[1] Herzog H, K Caldeira, J Reilly. An issue of permanence: Assessing the effectiveness of temporary carbon storage. Clim Change. 59 (2003) 293-310, doi: 10.1023/A:1024801618900.

[2] Metz B, O Davidson, H De Coninck, M Loos, L Meyer. IPCC, 2005: IPCC special report on carbon dioxide capture and storage. Prepared by Working Group III of the

Intergovernmental Panel on Climate Change. Cambridge, United Kingdom and New York, NY, USA, 442 pp. (2005).
[3] Langmuir D, P Hall, J Drever. Environmental Geochemistry. Prentice Hall, New Jersey, 1997.
[4] Morse JW, FT Mackenzie. Geochemistry of sedimentary carbonates. (1990).
[5] Peng C, JP Crawshaw, GC Maitland, JM Trusler, D Vega-Maza. The pH of CO 2-saturated water at temperatures between 308K and 423K at pressures up to 15MPa. J Supercrit Fluid. 82 (2013) 129-37, doi: 10.1016/j.supflu.2013.07.001.
[6] Peng C, JP Crawshaw, GC Maitland, JM Trusler. Kinetics of calcite dissolution in CO 2-saturated water at temperatures between (323 and 373) K and pressures up to 13.8 MPa. Chem Geol. 403 (2015) 74-85, doi: 10.1016/j.chemgeo.2015.03.012.
[7] Mohamed IM, HA Nasr-El-Din. Formation Damage Due to CO2 Sequestration in Deep Saline Carbonate Aquifers. SPE International Symposium and Exhibition on Formation Damage Control. Society of Petroleum Engineers2012.
[8] Birkholzer JT, JP Nicot, CM Oldenburg, QL Zhou, S Kraemer, K Bandilla. Brine flow up a well caused by pressure perturbation from geologic carbon sequestration: Static and dynamic evaluations. Int J Greenh Gas Con. 5 (2011) 850-61, doi: 10.1016/j.ijggc.2011.01.003.
[9] Daccord G, R Lenormand, O Lietard. Chemical Dissolution of a Porous-Medium by a Reactive Fluid .1. Model for the Wormholing Phenomenon. Chem Eng Sci. 48 (1993) 169-78, doi: 10.1016/0009-2509(93)80293-y.
[10] Daccord G, O Lietard, R Lenormand. Chemical Dissolution of a Porous-medium by a Reactive Fluid .2. Convection vs Reaction, Behavior Diagram. Chem Eng Sci. 48 (1993) 179-86, doi: 10.1016/0009-2509(93)80294-z.
[11] Maheshwari P, R Ratnakar, N Kalia, V Balakotaiah. 3-D simulation and analysis of reactive dissolution and wormhole formation in carbonate rocks. Chem Eng Sci. 90 (2013) 258-74, doi: 10.2118/171731-PA.
[12] El-Maghraby R, C Pentland, S Iglauer, M Blunt. A fast method to equilibrate carbon dioxide with brine at high pressure and elevated temperature including solubility measurements. J Supercrit Fluid. 62 (2012) 55-9, doi: 10.1016/j.supflu.2011.11.002.
[13] Fredd C, S Fogler. Influence of Transport and Reaction on Wormhole Formations in Porous Media. AIChE. 44 (1998), doi: 10.1002/aic.690440902.
[14] Luquot L, P Gouze. Experimental determination of porosity and permeability changes induced by injection of CO2 into carbonate rocks. Chem Geol. 265 (2009) 148-59, doi: 10.1016/j.chemgeo.2009.03.028.
[15] Li L, CA Peters, MA Celia. Upscaling geochemical reaction rates using pore-scale network modeling. Adv Water Resour. 29 (2006) 1351-70, doi: 10.1016/j.advwatres.2005.10.011.
[16] Rötting TS, L Luquot, J Carrera, DJ Casalinuovo. Changes in porosity, permeability, water retention curve and reactive surface area during carbonate rock dissolution. Chem Geol. 403 (2015) 86-98, doi: 10.1016/j.chemgeo.2015.03.008.
[17] Fredd C, H Fogler. Optimum conditions for wormhole formation in carbonate porous media: Influence of transport and reaction. SPE Journal. 4 (1999) 196-205.
[18] Mettler Jr FA, PW Wiest, JA Locken, CA Kelsey. CT scanning: patterns of use and dose. J Radiol Prot. 20 (2000) 353.

[19] Ritman EL. Micro-computed tomography-current status and developments. Annu Rev Biomed Eng. 6 (2004) 185-208.
[20] Ott H, K de Kloe, M van Bakel, F Vos, A van Pelt, P Legerstee, et al. Core-flood experiment for transport of reactive fluids in rocks. Rev Sci Instrum. 83 (2012) 084501, doi: 10.1063/1.4746997.
[21] Ellis B, C Peters, J Fitts, G Bromhal, D McIntyre, R Warzinski, et al. Deterioration of a fractured carbonate caprock exposed to CO2 - acidified brine flow. Greenhouse Gases: Science and Technology. 1 (2011) 248-60.
[22] Smith MM, Y Sholokhova, Y Hao, SA Carroll. Evaporite caprock integrity: An experimental study of reactive mineralogy and pore-scale heterogeneity during brine-CO2 exposure. Environ Sci Technol. 47 (2012) 262-8.
[23] Lamy - Chappuis B, D Angus, Q Fisher, C Grattoni, BW Yardley. Rapid porosity and permeability changes of calcareous sandstone due to CO2 - enriched brine injection. Geophys Res Lett. 41 (2014) 399-406.
[24] Noiriel C, P Gouze, B Made. 3D analysis of geometry and flow changes in a limestone fracture during dissolution. J Hydrol. 486 (2013) 211-23, doi: 10.1016/j.jhydrol.2013.01.035.
[25] Noiriel C, P Gouze, D Bernard. Investigation of porosity and permeability effects from microstructure changes during limestone dissolution. Geophys Res Lett. 31 (2004).
[26] Menke HP, B Bijeljic, MG Andrew, MJ Blunt. Dynamic Three-Dimensional Pore-Scale Imaging of Reaction in a Carbonate at Reservoir Conditions. Environ Sci Technol. 49 (2015) 4407-14, doi: 10.1021/es505789f.
[27] Menke HP, B Bijeljic, MJ Blunt. Reservoir Condition Imaging of Reactive Transport in Heterogeneous Carbonates Using Fast Synchrotron Tomography – Effect of Initial Pore structure and Flow Conditions. Chem Geol. 428 (2016) 15-26, doi: 10.1016/j.chemgeo.2016.02.030.
[28] Menke HP, B Bijeljic, MJ Blunt. Dynamic Reservoir-Condition Microtomography of Reactive Transport in Complex Carbonates using a Laboratory Source: Effect of Initial Pore structure and Reactive Conditions. Geochim Cosmochim Acta. (2016), doi: IN REVIEW.
[29] Reynolds CA, S Krevor. Characterizing flow behavior for gas injection: Relative permeability of CO2 - brine and N2 - water in heterogeneous rocks. Water Resour Res. 51 (2015) 9464-89, doi: 10.1002/2015WR018046.
[30] Krevor SC, R Pini, B Li, SM Benson. Capillary heterogeneity trapping of CO2 in a sandstone rock at reservoir conditions. Geophys Res Lett. 38 (2011) L15401.

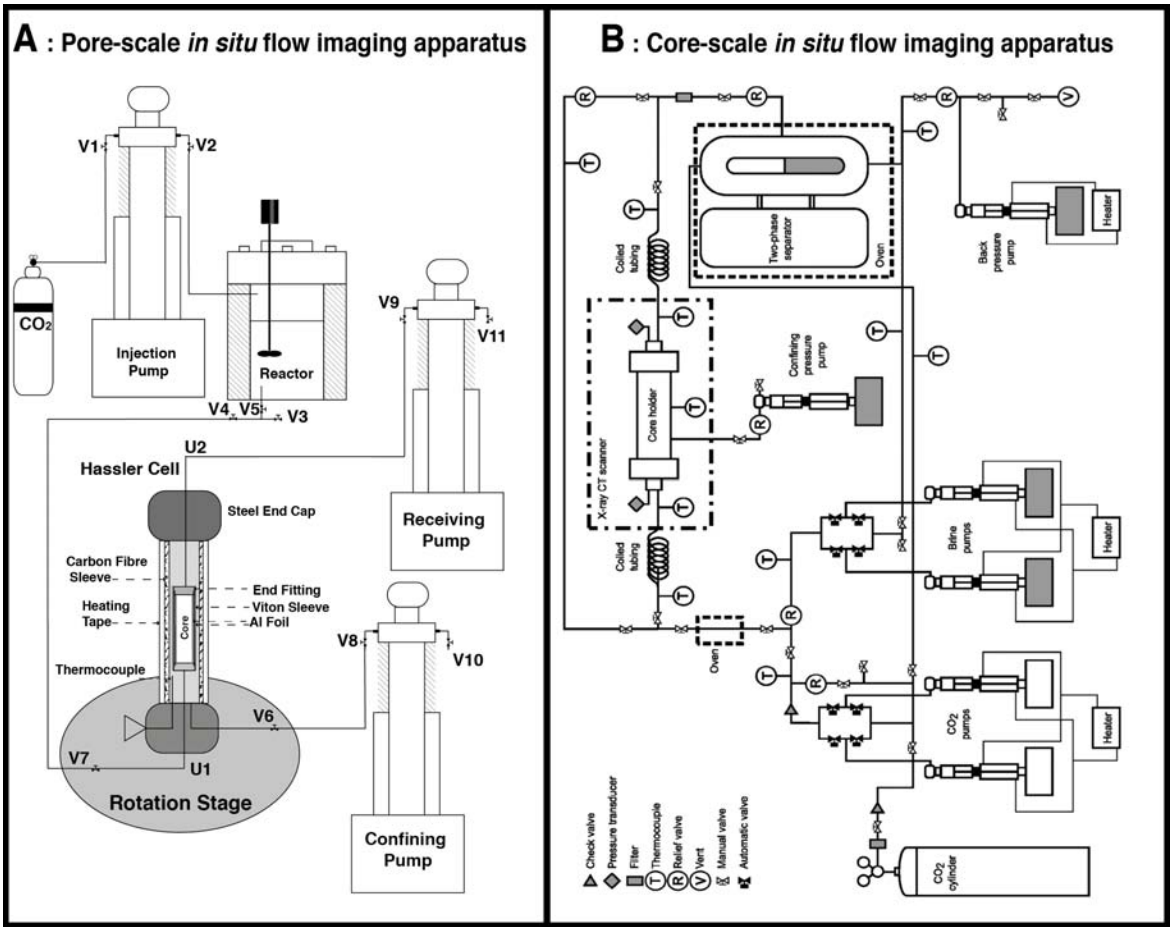

Figure 1: The pore (A) and core (B) scale flow and imaging apparatuses which show how high pressure syringe pumps were connected to the flow cells to assemble the *in situ* experimental apparatuses. In the pore scale apparatus (A) CO_2 is pressurized by the injection pump and used to equilibrate brine in the reactor. Reactive brine is pulled through core assembly by the receiving pump. The cell is confined by deionized water in the confining pump and heated using heating tape controlled by a thermocouple in the confining fluid. The experimental system is connected together using tubing and fluid flow is directed using Valves (V) and Unions (U). Modified from Menke et al. [26]. In the core scale apparatus (B) CO_2 and brine are circulated using the bypass loop and two-phase separator to equilibrate the brine. Reactive brine is then pushed through the core assembly by the brine pumps. Pressure is measured by the pressure transducers on either side of the core and the cell is confined by deionised water in the confining pump. The entire system is heated using PID controlled heaters and thermocouples. Taken with permission from [29].

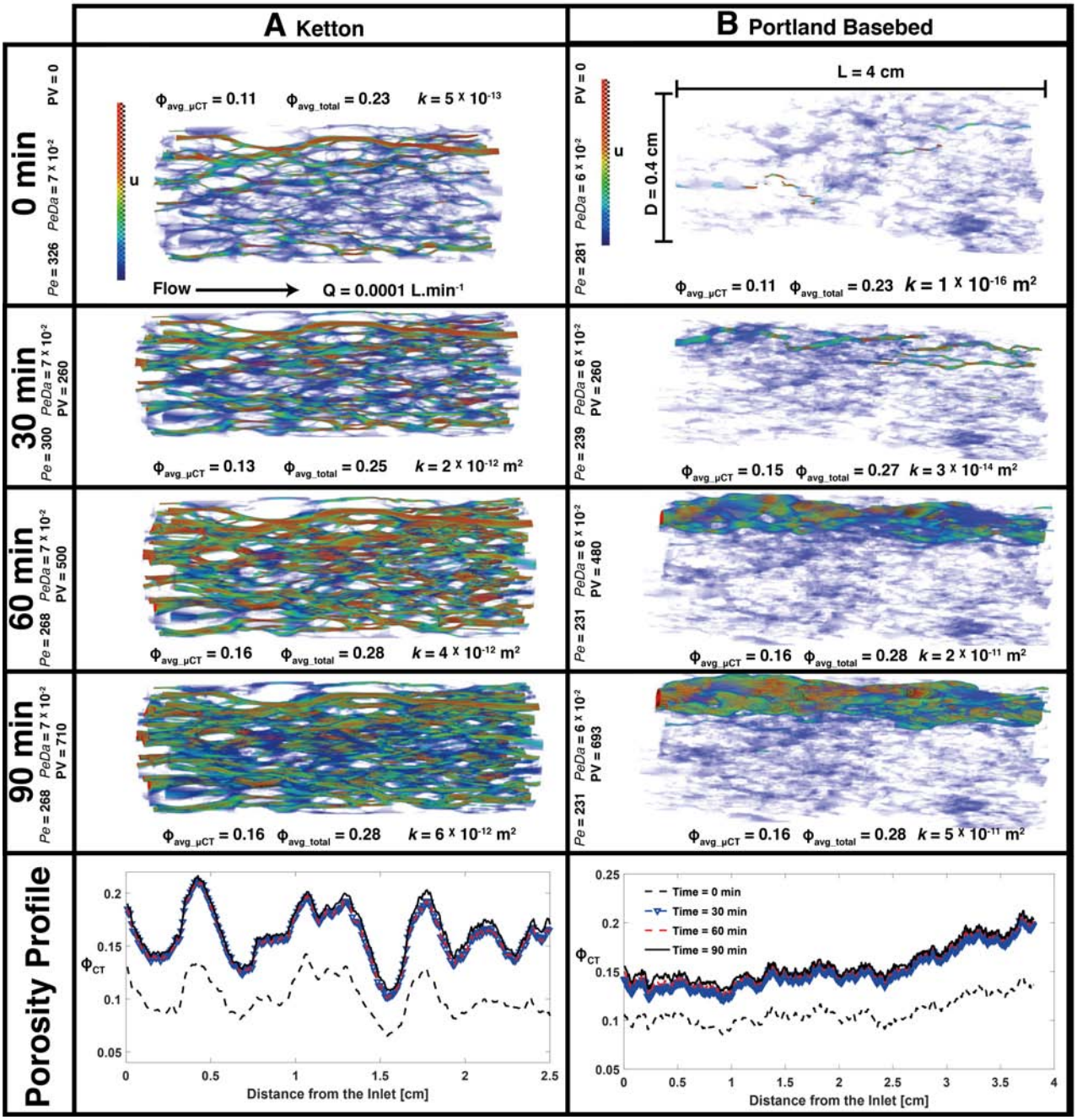

Figure 2: Pore scale porosity, permeability, and velocity evolution with time for Ketton (A) and Portland (B). Average porosity profiles along the direction of flow and connected porosity with high velocity regions are visualised for 0, 30, 60, and 90 minutes. High velocity regions are red. Connected porosity is blue. ϕ_{total} is calculated using $\phi_{avg\_total} = \phi_{grain}\ (1 - \phi_{avg\_CT}) + \phi_{avg\_CT}$ where the grain porosity ϕ_{grain} is estimated using the helium porosity for the first image and assumed constant for the duration of the experiments. *Pe* and *PeDa* are calculated according to the method presented in Menke et al. [26] using ϕ_{avg_total}. *PV* represents the number of pore volumes of brine to pass through the sample.

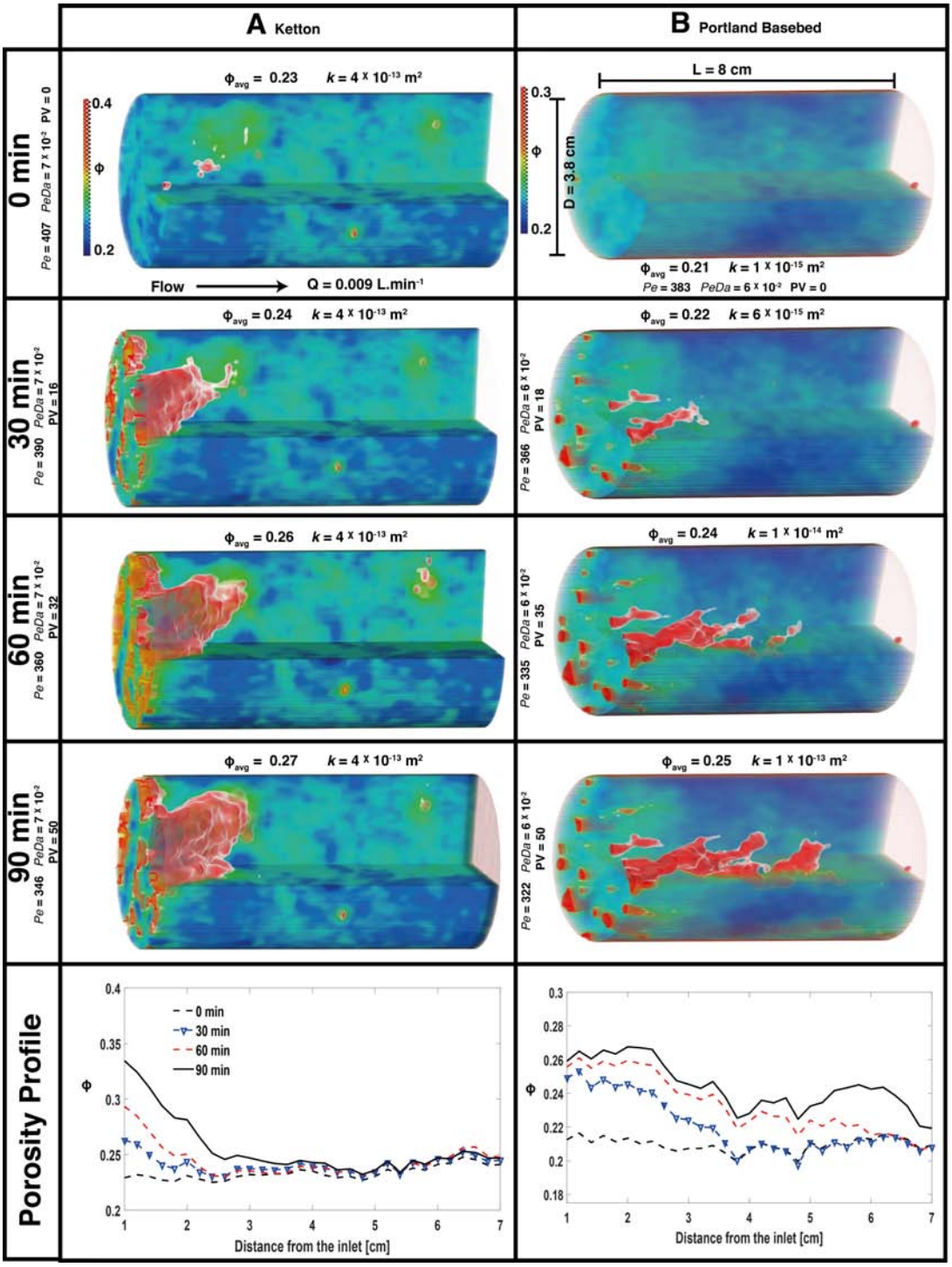

Figure 3: Core scale porosity and permeability evolution with time for Ketton (A) and Portland (B). Porosity profiles along the direction of flow and porosity are visualised for 0, 30, 60, and 90 minutes. High porosity regions are red and low porosity regions are blue. *Pe* and *PeDa* are calculated according to the method presented in Menke et al. [26] using ϕ_{avg}.

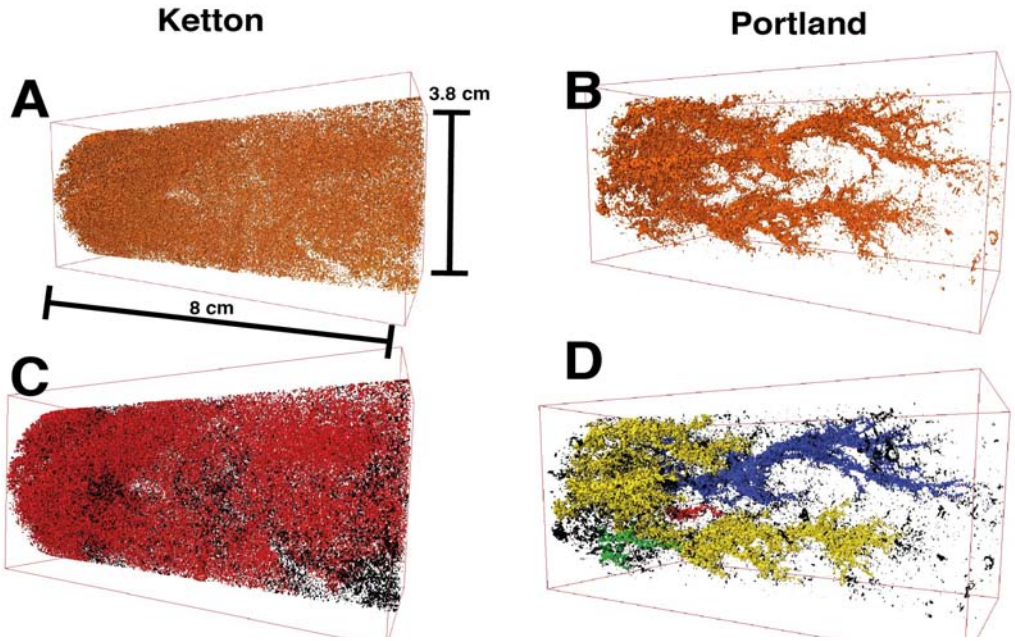

Figure 4: Pore space renderings of Ketton (A) and Portland (B) macro cores. The connected channels (coloured) are shown separated from the unconnected pore space (black) for Ketton (C) and Portland (D).

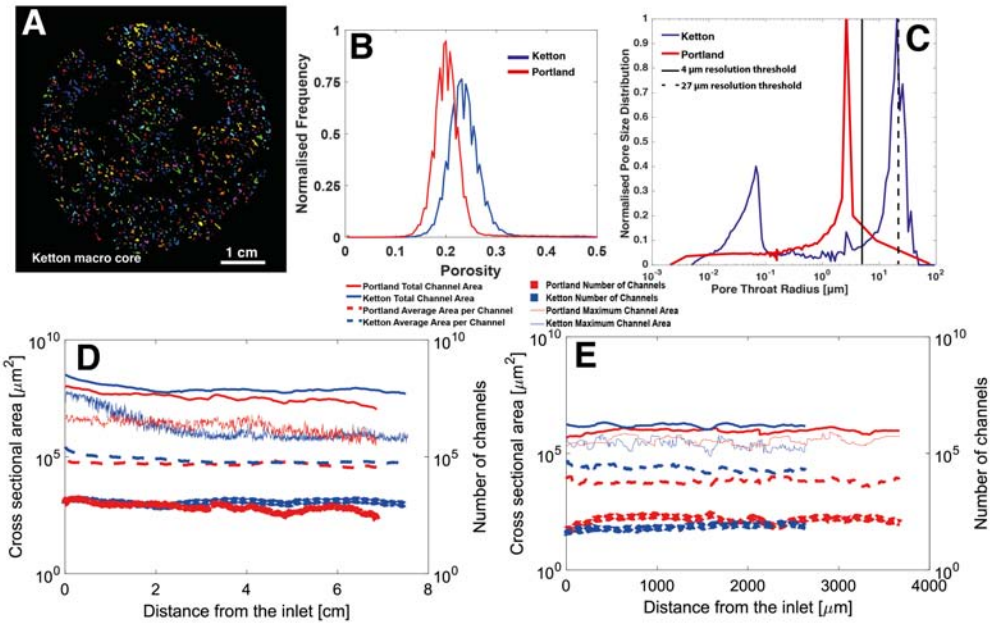

Figure 5: A segmented slice of post-reaction Ketton (A) perpendicular to the axis of flow labelled by individual channel. The normalised porosity frequency of the unreacted core scale samples is shown in B. The normalised pore size distributions (C) for Ketton (blue) and Portland (red) derived from MICP tests with the image resolution limits for 4 μm (solid) and 27 μm (dashed). The total cross sectional area, average cross sectional area, maximum cross sectional area and number of channels per slice along the axis of flow for the macro (D) and micro (E) core experiments.